ROBUST ESTIMATION OF THE VERTICAL STRUCTURE OF FORESTS WITH COHERENCE TOMOGRAPHY

Matteo Pardini and Konstantinos P. Papathanassiou

German Aerospace Center (DLR), 82234 Wessling, Germany
E-mail: matteo.pardini@dlr.de

ABSTRACT

SAR Tomography techniques with long wavelength acquisitions have demonstrated the capability of imaging the vertical structure of forests. In particular, Coherence Tomography (CT) is capable to estimate the low spatial frequency components of the vertical profile from a limited number of tracks, given the height boundaries in which the scattering occurs. However, the CT inversion procedure is sensitive to errors in such height boundaries and phase miscalibration residuals. In this paper, we propose a CT-based inversion robust to height and phase errors. A performance analysis is carried out with simulated data in a variety of scenarios, and first-cut results with real data are shown.

Key words: Synthetic aperture radar interferometry; tomography; robust processing.

1. INTRODUCTION

In the last decade, the accurate and reliable estimation of forest biomass has gained increasing attention within the SAR remote sensing community, given its crucial role in terrestrial carbon budget. First approaches for biomass estimation were based on the allometric relation between biomass and top canopy height [1]; however, the performance of such estimation is limited in forest systems with strong density variations. Recently, experimental evidence has suggested the possibility to extend the height to biomass allometry by considering the low spatial frequency components of the vertical biomass distribution function [2]. In the radar remote sensing framework, conventional SAR Tomography techniques have demonstrated the capability of imaging the vertical structure by exploiting the spatial (i.e. baseline) diversity of the acquisitions, possibly jointly with polarization diversity [3–6]. However, especially considering the implementation of space-borne missions, temporal decorrelation problems limit the number of suitable acquisition for the tomographic processing. For this reason, the Coherence Tomography (CT) technique has been recently proposed [7, 8]. In brief, CT aims at decomposing the vertical profile on a set of orthogonal basis functions through a least squares fitting with the available complex coherences (possibly obtained by combining different polarizations), after compensating them for the phase histories produced by the ground topography and the volume depth along the baselines. So doing, the tomographic reconstruction reduces to the estimation of the coefficients of the series and can be carried out with a low number of acquisitions. However, if the topography and the volume height are not estimated with sufficient accuracy, the related phase errors dramatically affect the CT inversion, with misleading results in terms of vertical profiles. The same effect shows up also in presence of phase non-idealities due to atmospheric propagation and inaccuracies in the relative radar platform position measurements between the acquisitions.

This work tackles the problem of the robust estimation of forest vertical profiles by means of CT in presence of the above mentioned phase errors. To counteract their effects, the proposed solution consists in relying as much as possible on the coherence amplitudes. It is demonstrated that with the coherence amplitudes the reliable LS estimation is possible of the absolute values of the Legendre coefficients; to estimate their signs, the coherence phases can be used. This two-step CT is expected to furnish more accurate results with respect to the original CT inversion at the complex level. The performance in profile estimation of the proposed algorithm will be analyzed in controlled conditions by means of simulated coherences, with reference to realistic vertical profiles, and pros and cons discussed. In addition, first-cut experimental results will be shown by using SAR data acquired with the DLR's E-SAR airborne sensor.

2. BASICS OF COHERENCE TOMOGRAPHY

We suppose to process a coherence data set in which only the vegetation contribution is present, i.e. without (or at least very reduced) ground backscattering. This can be achieved for instance by combining data with different polarizations, and by selecting the optimal polarization combination e.g. employing all the baselines and all the polarizations in a coherent processing [9]. Moreover, the *a priori* knowledge is needed regarding the volume depth

H and the ground topography z_0. If not available, these two quantities can be estimated from the data, possibily exploiting again different polarizations [10].

2.1. Vertical profile as a weighted sum of Legendre polynomials

Let $B(z)$ be the wanted vertical profile, where z denotes the vertical height dimension. The CT inversion is based on the fact that $B(z)$ can be expanded as a weighted sum of polynomials:

$$B(z) = \sum_n a_n P_n(z) \tag{1}$$

where a_n, $n = 0, 1, 2, \ldots$, are the expansion coefficients and $P_n(z)$ the polynomials. For a given baseline, corresponding to a vertical wavenumber k_z, this profile furnishes the following complex coherence:

$$\gamma(k_z) = e^{jk_z z_0} \frac{\int_0^H B(z) e^{jk_z z} dz}{\int_0^H B(z) dz}, \tag{2}$$

with $0 \leq \gamma(k_z) \leq 1$. As common [7], we consider the Legendre polynomials. For this purpose, the height axis needs to be scaled from $[z_0, z_0 + H]$ to $[-1, 1]$. The first Legendre polynomials are[1]:

$$\begin{array}{l} P_0(z) = 1 \\ P_1(z) = z \\ P_2(z) = (3z^2 - 1)/2 \\ P_3(z) = (35z^4 - 30z^2 + 3)/2 \end{array} \tag{3}$$

while in general it results [11]:

$$P_n(z) = \frac{2n-1}{n} z P_{n-1}(z) - \frac{n-1}{n} P_{n-2}(z). \tag{4}$$

In terms of coherence, after the height rescaling and by using the Legendre expansion, equation (2) can be written as

$$\gamma(k_z) = e^{jk_z z_0} e^{jk_V} \sum_n a_n f_n(k_V) \tag{5}$$

where $k_V = k_z H/2$ and $f_n(k_V) = \int_{-1}^{1} P_n(z) e^{jk_V z} dz$. The functions $f_n(k_V)$ can be calculated in closed form as follows:

$$\begin{cases} f_n(k_V) = \dfrac{2n-1}{jk_V} f_{n-1}(k_V) + f_{n-2}(k_V) \\ f_0(k_V) = 2\dfrac{\sin k_v}{k_V} \\ f_1(k_V) = 2j\left(\dfrac{\sin k_V}{k_V^2} - \dfrac{\cos k_V}{k_V}\right) \end{cases} \tag{6}$$

[1] With a slight abuse of notation, the re-scaled height axis is named again z for simplicity.

2.2. Legendre coefficients estimation

We suppose that a finite number of acquisitions are available, furnishing K non-zero baselines. No hypotheses are made regarding their spatial regularity. At the $k-$th baseline the coherence $\gamma(k_{z,k})$ is estimated and all the coherences are collected in the $K-$dimensional column vector $\boldsymbol{\gamma}$. Thus, supposing that N coefficients are of interest, CT aims at estimating the Legendre coefficient vector $\mathbf{a}$, where $[\mathbf{a}]_n = a_n$, $n = 0, \ldots, N$, given the coherence vector $\boldsymbol{\gamma}$, the volume depth H and the ground topography z_0.

Starting from the original formulation in [7], here we adopt a slightly different CT formulation which is based on a least squares (LS) fitting between the available coherences and the Legendre-reconstructed ones[2]. As a consequence, remembering that $a_0 = 1$ [7], the CT coefficients can be estimated by minimizing the following LS functional:

$$J = \sum_{k=1}^{K} \parallel \gamma_k - \gamma_{L,k} \parallel^2 = \parallel \boldsymbol{\gamma} - \boldsymbol{\gamma}_L \parallel^2 . \tag{7}$$

The vector $\boldsymbol{\gamma}_L$ of the Legendre-reconstructed coherences can be further expressed as a function of $f_n(k_{V,k})$ and $\mathbf{a}$. Following also the development in [7], for the $k-$th coherence lag define the $N \times 2$ matrix:

$$\mathbf{F}_k = \begin{bmatrix} f_1(k_{V,k}) & 0 & f_3(k_{V,k}) & \cdots \\ 0 & f_2(k_{V,k}) & 0 & \cdots \end{bmatrix} \tag{8}$$

and the $2-$dimensional vector:

$$\mathbf{b}_k = \begin{bmatrix} \Im\{\tilde{\gamma}_k\} \\ \Re\{\tilde{\gamma}_k\} - f_0(k_{z,k}) \end{bmatrix}, \tag{9}$$

where

$$\tilde{\gamma}_k = \gamma_k e^{-jk_{V,k}} e^{-jk_{z,k} z_0}. \tag{10}$$

After forming the following matrices:

$$\mathbf{F} = \begin{bmatrix} \mathbf{F}_1 \\ \vdots \\ \mathbf{F}_K \end{bmatrix}, \mathbf{b} = \begin{bmatrix} \mathbf{b}_1 \\ \vdots \\ \mathbf{b}_K \end{bmatrix}, \tag{11}$$

the functional in (7) can be rewritten as:

$$J = \parallel \mathbf{Fa} - \mathbf{b} \parallel^2 , \tag{12}$$

from which the coefficient vector is estimated after a minimization:

$$\hat{\mathbf{a}} = (\mathbf{F}^T \mathbf{F})^{-1} \mathbf{F}^T \mathbf{b}. \tag{13}$$

[2] From an algebraic point of view, it is worth noting that this LS formulation is the best criterion that can be adopted when the number of baselines is higher than the number of desired coefficients (overdetermined system of equations).

3. AMPLITUDE-BASED COHERENCE TOMOGRAPHY

As shown in (12), the coherence fitting is performed after the compensation of the phase history generated along the baselines by z_0 and H. However, errors in the estimation of z_0 and H introduce errors in the phase compensation (10)[3]. To reduce the effect of phase-related errors in the coherence, here we propose to use the coherence amplitudes. For the sake of brevity, in the following the proposed method will be named Amplitude-based CT (ACT). It is worth remarking that amplitude-only processing strategies have been already proposed in a tomographic-like context e.g. in [12] for the separation of point-like scatterers interfering in the same resolution cell in urban scenarios. However, the application to forest volumes is by far more challenging since continuous vertical profiles are to be estimated, while in the urban case only discrete scatterers parameters are of interest (e.g. the height and/or the deformation velocity). In addition, speaking in purely "tomographic" terms, it is well-known that the amplitude and phase information are both useful in order to exploit the modulation induced by the beating phenomena for the separation of the multiple signal components, and to possibly enhance statistical accuracy even for a single scatterer. This affirmation is true also for the proposed ACT, for which it is demonstrated that the coherence amplitudes are not enough to completely characterize all the expansion coefficients, but the phase is needed to estimate the sign of some of them.

More in detail, by further manipulating (5), we have

$$|\tilde{\gamma_k}|^2 = |\gamma_k|^2 \approx \sum_n a_n^2 |f_n(k_{V,k})|^2 + \\ + 2\sum_n \sum_{m \neq n} a_{2n} a_{2m} f_n(k_{V,k}) f_m(k_{V,k}) \quad (14)$$

for $2n, 2m \leq N$. Notice that the phase compensation is not needed anymore. The expression in (14) is composed by two terms, the second of which depends on the cross-products of the even order coefficients. As a consequence, it is apparent that from (14) the estimation is possibile of the absolute value only of the odd order coefficients and of absolute value and sign of the even order coefficients. Moreover, equation (14) is in principle complicated to be inverted. Nevertheless, for the application of interest we can assume $N = 3$ [2], in which case (14) becomes[4]:

$$|\gamma_k|^2 - |f_0(k_{V,k})|^2 \approx a_1^2 |f_1(k_{V,k})|^2 + a_2^2 |f_2(V_{z,k})|^2 + \\ + a_3^2 |f_3(k_{V,k})|^2 + 2a_2 f_0(k_{V,k}) f_2(k_{V,k}). \quad (15)$$

Extending (15) to all the available baselines, the following matrices and vector are introduced:

- $\mathbf{F}_0$: $(K, N)-$dimensional matrix with generic element $[\mathbf{F}_0]_{k,n} = |f_n(k_{V,k})|^2$;
- $\mathbf{F}_1$: $(K, N)-$dimensional matrix with elements $[\mathbf{F}_1]_{k,2} = 2 f_0(k_{V,k}) f_2(k_{V,k})$ and $[\mathbf{F}_1]_{k,n\neq 2} = 0$;
- $\boldsymbol{\gamma}'$: $K-$dimensional vector with generic element $[\boldsymbol{\gamma}']_k = |\gamma_k|^2 - |f_0(k_{V,k})|^2$,

and the coefficient vector can be estimated according to the following optimization criterion:

$$\hat{\boldsymbol{\alpha}} = \arg\min_{\boldsymbol{\alpha}} \|\mathbf{F}_0(\boldsymbol{\alpha} \odot \boldsymbol{\alpha}) + \mathbf{F}_1 \boldsymbol{\alpha} - \boldsymbol{\gamma}'\|^2, \quad (16)$$

where "$\odot$" indicates the Schur-Hadamard product, i.e. the element-by-element product, and

$$\boldsymbol{\alpha} = [\ |a_1| \quad a_2 \quad |a_3|\ ]^T. \quad (17)$$

As previously discussed, the optimization functional (16) is symmetric with respect to the axes $a_1 = 0$ and $a_3 = 0$, thus it allows the estimation of $|a_1|$ and $|a_3|$, while a_2 con be estimated with sign.

Coversely to the classical CT functional (12), the ACT functional (17) does not have a closed-form solution, as a consequence specific numerical procedures must be set up. A possibility is to distinguish between the estimation of $\boldsymbol{\alpha}_1 = [\ |a_1| \quad |a_3|\ ]^T$ and the estimation of a_2. In fact, if a_2 is known, then the optimization functional is linear in $\boldsymbol{\alpha}_1 \odot \boldsymbol{\alpha}_1$, which can thus be estimated in closed form. The suggested iterative relaxation procedure is composed by the following steps:

1. *Initialization*. Suppose that an initial value for a_2 is available, namely $\hat{a}_2[0]$. (*i*) Calculate $\bar{\boldsymbol{\gamma}}[0]$ by subtracting from $\boldsymbol{\gamma}'$ the coherence contribution related to $\hat{a}_2[0]$. (*ii*) Calculate the initial estimates $|\hat{a}_1[0]|$ and $|\hat{a}_3[0]|$ by means of the closed-form expressions reported in the Appendix.
2. *Iteration*. The $m-$th iteration is composed by two steps. (*i*) Compute an update $\hat{a}_2[m]$ from $\bar{\bar{\boldsymbol{\gamma}}}[m]$, which is calculated by subtracting from $\boldsymbol{\gamma}'$ the coherence contribution related to $|\hat{a}_1[m-1]|$ and $|\hat{a}_3[m-1]|$. (*ii*) Compute update estimates $|\hat{a}_1[m]|$ and $|\hat{a}_3[m]|$ from the coherence residual update $\bar{\boldsymbol{\gamma}}[m]$. Steps (*i*)-(*ii*) admit closed form expressions, as reported in the Appendix. To stop the iteration, a possibility is to require that the normalized distance between $\hat{\boldsymbol{\alpha}}[m]$ and $\hat{\boldsymbol{\alpha}}[m-1]$ is lower than a given threshold.

To estimate the signs of $\hat{a}_1$ and $\hat{a}_3$, which can not be furnished by (16), a simple strategy consists in using the coherence complex values. In other words, one can calculate the quantity J in (12) for $\hat{\boldsymbol{\alpha}}$ as a function of all the possible combinations of the signs of $\hat{a}_1$ and $\hat{a}_3$, and then choose the sign combination which minimizes J.

To conclude this Section, some important remarks are in order. First of all, we notice that the ACT functional (16) is in general different from the CT functional (12), and in principle they could give some slightly different coefficient estimates. Anyway, in our performance analysis

[3] It should be noted that errors in H will affect also the functions $f_n(k_{V,k})$, even if at lower extent [8]. Here, our objective is to develop an inversion algorithm robust against the more detrimental phase errors.

[4] Again, $a_0 = 1$.

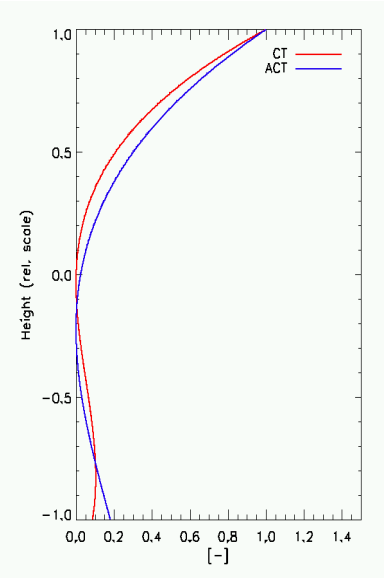

Figure 1. Vertical profiles estimated with CT and ACT in the reference scenario. The height axis is rescaled in the interval $[-1, 1]$.

(see Section 4) this difference has never been of particular concern. Second, the suggested iterative relaxation procedure requires a very low computational load. In fact, at each iteration, closed form expressions can be used; not only, but from experimental evidence a low number of iterations are required to reach the optimal coefficient vector. On the other hand, since functional (16) is in general not convex, the iterative procedure assures a convergence to a relative minimum (which is actually the result of any known iterative method). However, at each iteration the minimizing functional is convex, and admits a single minimum. Finally, concerning the number of baselines needed for the inversion, we recall that in the conventional complex CT inversion each baseline allow the estimation of two coefficients. For instance, in the specific case of $N = 3$, $K = 2$ is enough. On the other hand, to solve the ACT non-linear functional (16), a number of baseline $N \geq K$ is needed, thus reducing the amount of information which can be extracted from each baseline. This is reasonable, since in (16) only the amplitudes are used. However, $K = 2$ is sufficient to estimate $N = 3$ ACT coefficients thanks to the iterative procedure.

4. PERFORMANCE ANALYSIS WITH SIMULATED DATA

In this Section, the robustness in the Legendre coefficient estimation is analyzed for CT and ACT in presence of phase miscalibration residuals and errors in H and z_0. With reference to the typical parameters of an acquisition from an airborne platform (e.g. the DLR's E-SAR), we considered a dual baseline acquisition, with horizontal baselines measuring 5m and 20m with respect to the master track, radar carrier frequency 1.3GHz (L-band).

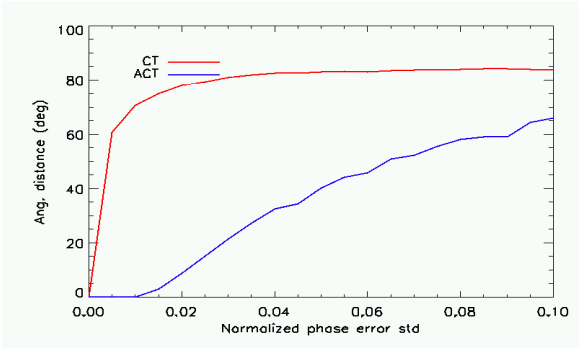

Figure 2. Angular distances as a function of the normalized phase error standard deviation.

In the reference scenario, the volume coherence has been modelled according to the RVOG model (i.e. with exponential vertical profile), with no ground contribution, ground height $z_0 = 0$m, volume depth $H = 20$m, extinction $\sigma = 0.2$dB/m, and look angle $\theta = 30°$ (near range). For this analysis, we will consider $N = 3$. In Fig. 1 the profiles estimated with CT and ACT are plotted in the reference scenario. The two profiles look very similar, although the difference in the respective functionals, as pointed out in Section 3. Since the Legendre polynomials constitute an orthogonal basis, in what follows the robustness has been assessed for each method in terms of the angular distance ϵ between the error-free coefficient vector $\mathbf{a}$ and the error corrupted one, namely $\mathbf{a}_e$. The higher ϵ, the lower the robustness level. In formulas:

$$\epsilon = \cos^{-1} \frac{\mathbf{a}^T \mathbf{a}_e}{\|\mathbf{a}\| \|\mathbf{a}_e\|} \tag{18}$$

In a first experiment, we tested the robustness of CT and ACT against phase miscalibration residuals. The miscalibrated coherence has been simulated as $\boldsymbol{\gamma}_e = \boldsymbol{\gamma} \odot \exp^{j4\pi\mathbf{d}}$, where $\mathbf{d}$ is a $K-$dimensional vector containing the residual baseline positioning estimation errors, normalized with respect to the wavelength λ. Vector $\mathbf{d}$ has been simulated as a Gaussian vector, whose elements are statistically independent random variables with standard deviation δ (in λ units). For instance, $\delta = 0.04$ corresponds to a phase error which is contained in the interval $[-30°, 30°]$ with probability around 66%. The angular distances averaged over 100 realizations of $\mathbf{d}$ are reported in Fig. 2 as a function of δ. It is apparent that CT is extremely sensitive to such errors, furnishing $\epsilon = 30°$ already with $\delta = 0.0025$, a very low value. ACT is still sensistive, but it shows a much higher degree of robustness, with ϵ approaching $30°$ with δ around 0.04. It is worth noting that for ACT the increase of ϵ is due in errors in the estimation of the coefficient signs, since $\mathbf{d}$ introduces pure phase errors in the coherence. It has been verified (again by simulation) that this residual sensitivity of ACT can be mitigated by adding baselines to the input data set, so that the degree of fitting in (12) is augmented in the final step of the inversion.

The estimation robustness has been tested also for dif-

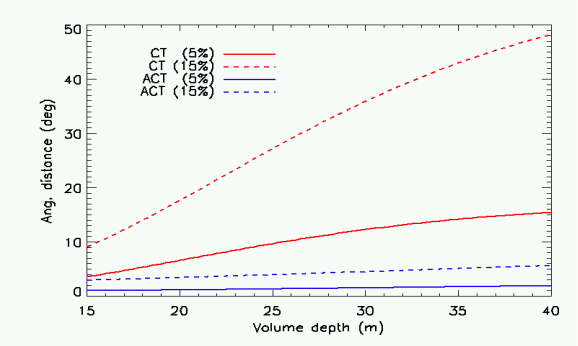

(a) With errors in H

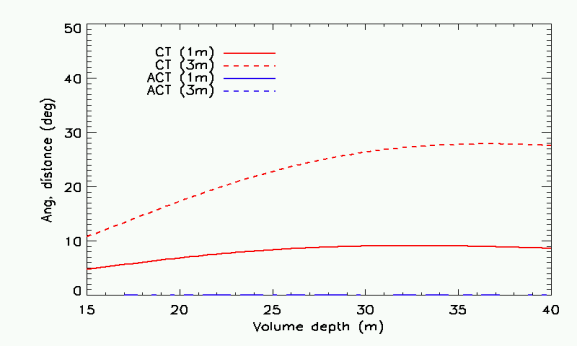

(b) With errors in z_0

Figure 3. Angular distances as a function of the volume depth H.

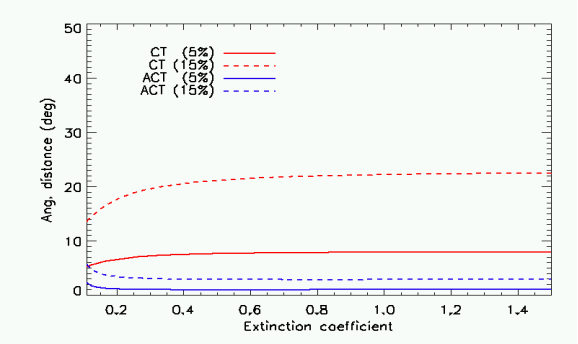

(a) With errors in H

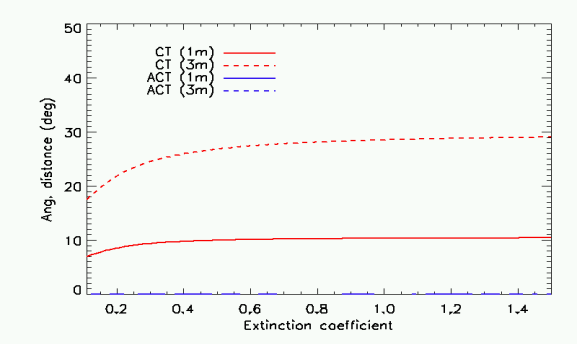

(b) With errors in z_0

Figure 4. Angular distances as a function of the volume extinction.

ferent forest scenarios, i.e. by varying one per time the RVOG parameters H and σ. In Fig. 3, ϵ is reported as a function of H for different H errors [Fig. 3(a)] and for different z_0 errors [Fig. 3(b)], namely ΔH and Δz_0, respectively, assumed as deterministic quantities in these experiments. We considered $\Delta H = 5\%$ and $\Delta H = 15\%$. From Fig. 3(a), we observe that increasing levels of ΔH turn out in increasing ϵ for both CT and ACT. Regarding CT, ϵ is steadily increasing at the increase of H since the absolute height errors increases, and the most critical case is for $\Delta H = 15\%$. On the contrary, ACT shows its robustness, with $\epsilon < 5^\circ$ and very slowly increasing at the increase of H also for $\Delta H = 15\%$. The residual ϵ is due to the errors that ΔH induces on the computation of the functions $f_n(k_{V,k})$. Concerning the errors in the topography, we assumed $\Delta z_0 = 1$m (which is in the order of magnitude of the accuracy limit predicted by the Cramér-Rao lower bound) and $\Delta z_0 = 3$m. We recall that the topography error only induce phase compensation errors in the coherences [see (10)]. From Fig. 3(b), it is apparent that CT is very sensitive to the presence of a non-null Δz_0, even if for large volumes its effect tends to reduce as Δz_0 becomes negligible with respect to H in (10). On the other hand, at least in the considered case studies, ACT inversion is independent from Δz_0, also with this very low number of baselines. In Fig. 4, ϵ is reported as a function of the extinction σ for both methods in presence of volume depth and topography errors. Again, we observe an increased robustness of ACT with respect to CT, especially regarding in the case of not well-known topography.

The final case study analyses how the robustness is dependent on the look-angle θ in the forest scenario of reference and given the same horizontal baselines. Recalling (10), at the increase of θ we expect the sensitivity to ΔH and Δz_0 to reduce, as k_z reduces. This analysis is reported in Fig. 5, in which ϵ is reported for a look angle variation typical of an airborne acquisition from near to far range. For the sake of simplicity, we hypothesized to observe a flat terrain, without slope variations. The simulations confirm the expectancies: H and z_0 errors impact at a higher extent in near range, although ACT profile estimation is rather independent from their presence.

5. FIRST-CUT RESULTS WITH REAL DATA

A first analysis of the behaviour of ACT in presence of height errors has been carried out also with real data. We considered a DLR's E-SAR dataset over the Traunstein forest site in the south of Germany, next to the city Traunstein. The acquisition campaign was carried out in June 2008, with a time span of 1 hour. The dataset consist of 5 fully polarimetric SAR images in L-band, with nominal uniform spaced baselines from 0 to 20m. The topography varies from $530 - 650$m amsl, with only few steep slopes; forest heigth is in average higher than 20m. For both topography and forest height LiDAR measurements are available.

In our experiment, the reference profiles (*viz.* error-free)

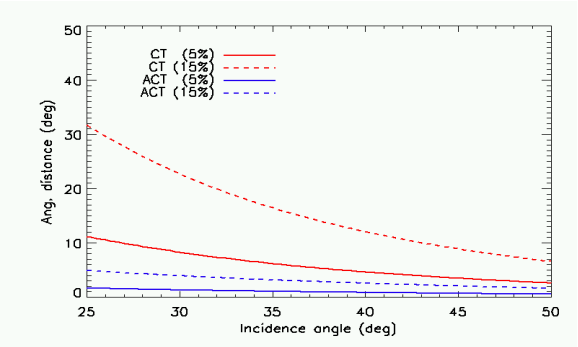

(a) With errors in H

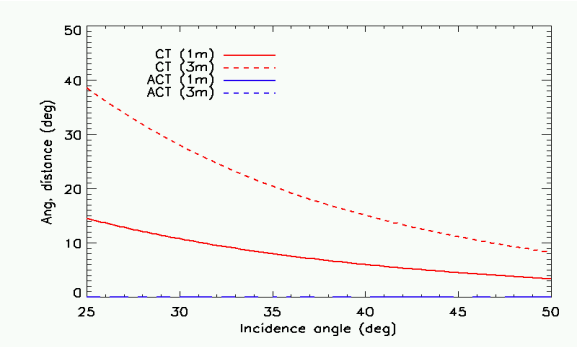

(b) With errors in z_0

Figure 5. Angular distances as a function of the look angle.

are those calculated by exploiting the LiDAR z_0 and H. In Fig. 6 the ACT tomographic slice is reported in the height-range plane for a fixed azimuth coordinate and HV polarization; heights are relative to the flat-earth reference height. Vertical profiles are imaged between the z_0 and H at each range coordinate where LiDAR measurements are available. The imaged forest stands are rather tall, in general taller than 20m, with a peak height around 40m between the range bins 400 and 600. The main scattering constributions are located close to the canopy top, as it is reasonable to expect from L-band data.

The robustness against topography and forest height errors has been evaluated for both CT and ACT by adding height errors to the LiDAR measurements. Errors have been simulated as zero-mean Gaussian random variables independent from range bin to range bin; the robustness has been measured by calculating the average ϵ over 500 realizations. In Fig. 7(a), the average ϵ is plotted with H errors with standard deviation amounting to the 15%. ACT demonstrates a much improved robustness to height errors than CT, with average ϵ in general lower than 20°, with values consistent with those found in the simulated analysis. Fig. 7(b) reports the average ϵ with z_0 errors (standard deviation 1m). Again, the ACT performance does not suffer from topography errors, at least at this azimuth coordinate.

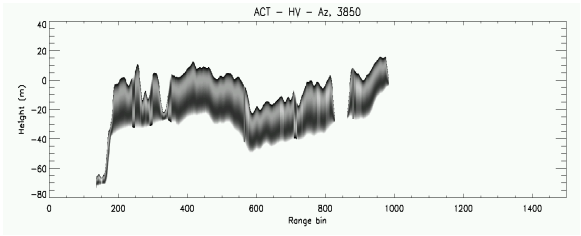

Figure 6. Vertical profiles estimated with ACT in the height-range plane.

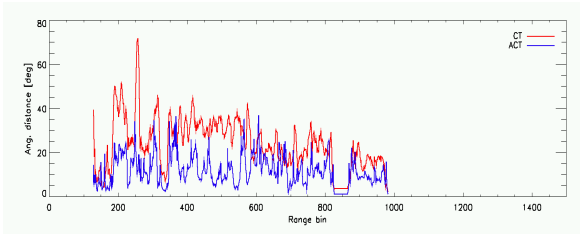

(a) With errors in H

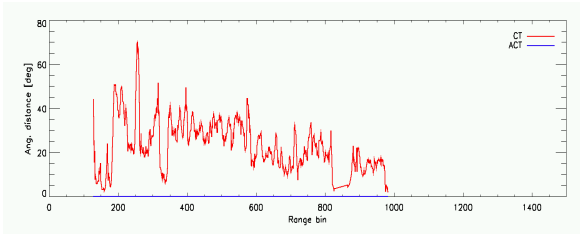

(b) With errors in z_0

Figure 7. Angular distances as a function of the range bin.

6. CONCLUSIONS

In this work, we proposed a CT-based inversion for the derivation of the vertical structure of forests from multibaseline SAR data. The proposed technique, which has been named Amplitude-based CT (ACT) has been designed to be robust against errors in estimation of the height boundaries in which the scattering occurs and phase miscalibration residuals. The proposed ACT uses the multibaseline complex coherences in two "incoherent processing" steps. In a first step, the coherence amplitudes are employed to estimate the absolute values of the expansion coefficients of the vertical profile in the Legendre polynomials basis; in the second step, the coherence phases are used to estimate the coefficient signs. It is worth noting that for the proposed inversion no closed-form formulas are available in general. However, if the first 3 coefficients are of interest (as in the case of structure-based biomass estimation [2]), it has been demonstrated that a fast and reliable iterative relaxation procedure can be adopted. The robustness performance of the proposed inversion has been measured by means of simulated and real data in a variety of forest scenarios. ACT has been shown to be more robust than the conventional CT. Future work could regard further experiment-

ing the proposed method with real data.

APPENDIX

In this Appendix, closed-form formulas are given for the iterative optimization of functional (16). As observed in Section 3, we can employ a relaxation-based procedure, in which each step has closed-form expression for the otputs, noticeably reducing the computational load. Two sub-problems must then be solved:

1. the estimation of $|a_1|$ and $|a_3|$ given a_2;
2. the estimation of a_2 given $|a_1|$ and $|a_3|$.

Estimation of $|a_1|$ and $|a_3|$ given a_2

In this case, equation (15) can be rewritten as:

$$|\gamma_k|^2 - |f_0(k_{V,k})|^2 - a_2^2|f_2(k_{V,k})|^2 + \\ -2a_2 f_0(k_{V,k}) f_2(k_{V,k}) \approx a_1^2|f_1(k_{V,k})|^2 + a_3^2|f_3(k_{V,k})|^2. \quad (19)$$

Define the following matrices and vectors:

- the $(K,2)-$dimensional matrix $\mathbf{F}_2$ with column elements $[\mathbf{F}_2]_{k,1} = |f_1(k_{V,k})|^2$ and $[\mathbf{F}_2]_{k,2} = |f_3(k_{V,k})|^2$;
- the $K-$dimensional vector $\bar{\boldsymbol{\gamma}}$, with $[\bar{\boldsymbol{\gamma}}]_k = |\gamma_k|^2 - |f_0(k_{V,k})|^2 - a_2^2|f_2(k_{V,k})|^2 - 2a_2 f_0(k_{V,k}) f_2(k_{V,k})$;
- the $2-$dimensional vector $\boldsymbol{\alpha}_1 = [\ |a_1| \quad |a_3|\ ]^T$.

As a consequence, $\boldsymbol{\alpha}_1$ can be estimated as:

$$\hat{\boldsymbol{\alpha}_1} = \arg\min_{\boldsymbol{\alpha}_1} \bar{J}(\boldsymbol{\alpha}_1) = \\ = \arg\min_{\boldsymbol{\alpha}_1} \| \mathbf{F}_1\boldsymbol{\alpha}_1 - \bar{\boldsymbol{\gamma}} \|^2 \text{ subject to } \boldsymbol{\alpha}_1 > 0 \quad (20)$$

in which the non-negativity constraint on the unknowns is needed since they are squared quantities, thus positive by definition. In the light of this, two case must be considered. If the constraint is not binding, then the solution to (20) is trivial and it is equal to

$$\hat{\boldsymbol{\alpha}}_1 = (\mathbf{F}_1^T\mathbf{F}_1)^{-1}\mathbf{F}_1^T\bar{\boldsymbol{\gamma}}, \quad (21)$$

and finally $|a_1| = \sqrt{[\hat{\boldsymbol{\alpha}}_1]_1}$ and $|a_3| = \sqrt{[\hat{\boldsymbol{\alpha}}_1]_2}$. On the other hand, if the constraint is binding, then one or both elements of $\hat{\boldsymbol{\alpha}}_1$ from (21) are negative. It is easy to recognize that functional (20) is a 2-D parabolic functional in the unknowns, thus it is convex in $\hat{\boldsymbol{\alpha}}_1$ and admits a single global minimum. It follows that if the constraint is binding, then the minimum will lie on the axes $a_1 = 0$ or $a_3 = 0$. For this reason, we can proceed in 4 steps: (1) suppose $a_1 = 0$ and find an estimate of a_3, obtaining a candidate solution $\hat{\boldsymbol{\alpha}}_{1,1}$; (2) suppose $a_3 = 0$ and find an estimate of a_1, obtaining a candidate solution $\hat{\boldsymbol{\alpha}}_{1,2}$; (3) calculate $\bar{J}(\hat{\boldsymbol{\alpha}}_{1,1})$ and $\bar{J}(\hat{\boldsymbol{\alpha}}_{1,2})$; (4) determine the optimal solution: $\hat{\boldsymbol{\alpha}}_1 = \hat{\boldsymbol{\alpha}}_{1,1}$ if $\bar{J}(\hat{\boldsymbol{\alpha}}_{1,1}) < \bar{J}(\hat{\boldsymbol{\alpha}}_{1,2})$, $\hat{\boldsymbol{\alpha}}_1 = \hat{\boldsymbol{\alpha}}_{1,2}$ vice versa. Concerning steps (1) and (2), the value of the non-null parameter can be determined in closed fom. For the sake of notation convenience, call χ the unknown parameter to be estimated ($|a_1|$ or $|a_3|$), and $\mathbf{f}$ the related column of $\mathbf{F}_2$ (the first or the second, respectively). As a consequence, the resulting $\bar{J}$ is a second degree equation whose solution is (taking into account also the non-negativity constraint):

$$\hat{\chi} = \begin{cases} \chi_0, & \text{if } \chi_0 \geq 0 \\ 0, & \text{if } \chi_0 < 0 \end{cases} \quad (22)$$

where

$$\chi_0 = \frac{\bar{\boldsymbol{\gamma}}^T\mathbf{f}}{\mathbf{f}^T\mathbf{f}}. \quad (23)$$

Moreover, it results:

$$\bar{J}([\hat{\chi}, 0]) = \begin{cases} \dfrac{\mathbf{f}^T\mathbf{f}\bar{\boldsymbol{\gamma}}^T\bar{\boldsymbol{\gamma}} - (\bar{\boldsymbol{\gamma}}^T\mathbf{f})^2}{\bar{\boldsymbol{\gamma}}^T\bar{\boldsymbol{\gamma}}}, & \text{if } \chi_0 \geq 0 \\ \bar{\boldsymbol{\gamma}}^T\bar{\boldsymbol{\gamma}}, & \text{if } \chi_0 < 0 \end{cases}. \quad (24)$$

Estimation of a_2 given $|a_1|$ and $|a_3|$

In this case, by adopting the notation introduced in this Appendix, and by introducing also the vectors $\mathbf{f}_1$ and $\mathbf{f}_2$ with elements, respectively, $[\mathbf{f}_1]_k = |f_2(kV,k)|^2$ and $[\mathbf{f}_2]_k = 2f_0(k_{V,k})f_2(k_{V,k})$, we can write the system of equation of the kind of (19) for all the baselines as:

$$\boldsymbol{\gamma}' - \mathbf{F}_2\boldsymbol{\alpha}_1 \approx a_2^2\mathbf{f}_1 + a_2\mathbf{f}_2. \quad (25)$$

As a consequence, by posing $\bar{\bar{\boldsymbol{\gamma}}} = \boldsymbol{\gamma}' - \mathbf{F}_2\boldsymbol{\alpha}_1$, a_2 can be estimated (with sign) as

$$\hat{a_2} = \arg\min_{a_2} \bar{\bar{J}}(a_2) = \\ = \arg\min_{a_2} \| \bar{\bar{\boldsymbol{\gamma}}} - a_2^2\mathbf{f}_1 - a_2\mathbf{f}_2 \|^2. \quad (26)$$

After simple but tedious algebraic manipulations, it results:

$$\bar{\bar{J}}(a_2) = c_4a_2^4 + c_3a_2^3 + c_2a_2^2 + c_1a_2 + c_0, \quad (27)$$

where $c_0 = \bar{\bar{\boldsymbol{\gamma}}}^T\bar{\bar{\boldsymbol{\gamma}}}$, $c_1 = -2\mathbf{f}_2^T\bar{\bar{\boldsymbol{\gamma}}}$, $c_2 = \mathbf{f}_2^T\mathbf{f}_2 - 2\mathbf{f}_1^T\bar{\bar{\boldsymbol{\gamma}}}$, $c_3 = 2\mathbf{f}_1^T\mathbf{f}_2$ and $c_4 = \mathbf{f}_1^T\mathbf{f}_1$. The minimum of $\bar{\bar{J}}(a_2)$ is found by calculating its derivative with respect to a_2 and by posing it equal to 0. Such derivative corresponds to a third order polynomial whose zeros can be calculated in closed-form [13].

REFERENCES

1. Mette T., Papathanassiou K., *et al.* (2004). Applying a common allometric equation to convert forest height from Pol-InSAR data to forest biomass. *Proc. of IEEE Int. Geosci. and Remote Sensing Symp.*

2. Toraño Caicoya A., Kugler F., *et al.* (2010). Biomass estimation as a function of vertical forest structure and forest height. Potential and limitations for radar remote sensing. *Proc. of EUSAR*.

3. Lombardini F., Pardini M. (2009). Experiments of tomography-Based SAR techniques with P-Band polarimetric data. *Proc. of ESA Polinsar*.

4. Nannini M., Scheiber R., *et al.* (2009). Estimation of the minimum number of tracks for SAR Tomography. *IEEE Trans. on Geosci. and Remote Sensing*, **47**(2).

5. Sauer S., Kugler F., *et al.* (2010). Polarimetric decomposition applied to 3D SAR images of forested terrains. *Proc. of EUSAR*.

6. Frey O., Meier E. (2010). Analyzing tomographic SAR data of a forest with respect to frequency, polarization and focusing technique. *Proc. of IEEE Int. Geosci. and Remote Sensing Symp.*

7. Cloude S. R. (2006). Polarization coherence tomography. *Radio Science*, **41**(4).

8. Cloude S. R. (2010). Forest vertical structure from P/L band spaceborne POLInSAR. *Proc. of EUSAR*.

9. S. Tebaldini (2009). Algebraic synthesis of forest scenarios from multibaseline PolInSAR data. *IEEE Trans. on Geosci. and Remote Sensing*, **47**(12).

10. Cloude S. R., Papathanassiou K. (1998). Polarimetric SAR Interferometry. *IEEE Trans. on Geosci. and Remote Sensing*, **36**(5).

11. Gilbert E. G., Otterman J., *et al.* (1960). A tabulation of Fourier transforms of trigonometric functions and Legendre polynomials. *Technical report*, University of Michigan.

12. Adam N., Bamler R., *et al.* (2005). Parametric estimation and model selection based on amplitude-only data in PS-Interferometry. *Proc. of ESA FRINGE*.

13. Weisstein E. W. (2010). Cubic formula. *MathWorld - A Wolfram Web Resource*, http://mathworld.wolfram.com/CubicFormula.html.